

ON THE ANOMALOUSLY LARGE EXTENSION OF THE PULSAR WIND NEBULA HESS J1825–137

DMITRY KHANGULYAN,^{1,2} ALEXANDER V. KOLDOBA,³ GALINA V. USTYUGOVA,^{3,4} SERGEY V. BOGOVALOV,⁵ AND
FELIX AHARONIAN^{6,7,5}

¹*Department of Physics, Rikkyo University, Nishi-Ikebukuro 3-34-1, Toshima-ku, Tokyo 171-8501, Japan*

²*RIKEN iTHEMS, Hirosawa 2-1, Wako, Saitama 351-0198, Japan*

³*Moscow Institute of Physics and Technology, Institutskiy per. 9, Dolgoprudny, Russia*

⁴*Keldysh Institute of Applied Mathematics RAN, Miusskaya sq. 4, Moscow, Russia*

⁵*National Research Nuclear University (MEPHI), Kashirskoye shosse, 31, Moscow, Russia*

⁶*Dublin Institute for Advanced Studies, School of Cosmic Physics, 31 Fitzwilliam Place, Dublin 2, Ireland*

⁷*Max-Planck-Institut für Kernphysik, Saupfercheckweg 1, 69117 Heidelberg, Germany*

Abstract

The very high energy (VHE) gamma-ray emission reported from a number of pulsar wind nebulae (PWNe) is naturally explained by the inverse Compton (IC) scattering of multi-TeV electrons. On the other hand, the physical dimensions of some gamma-ray emitting PWNe significantly exceed the scales anticipated by the standard hydrodynamical paradigm of PWN formation. The most “disturbing” case in this regard is HESS J1825-137 which extends to distances $r \approx 35$ pc from the central pulsar. If the gamma-ray emission is indeed produced inside the plerion, but not by electrons which escaped the nebula and diffuse in the interstellar medium (ISM), the formation of such an anomalously extended plerion could be realized, in an extremely diluted environment with the hydrogen number density $n_{\text{ISM}} \leq 10^{-2} \text{ cm}^{-3}$. In this paper, we explore an alternative scenario assuming that the pulsar responsible for the formation of the nebula initially had a very short rotation period. In this case, the sizes of both the PWN and the surrounding SNR depend on the initial pulsar period, the braking index, and the ISM density. To check the feasibility of this scenario, we study the parameter space that would reproduce the size of HESS J1825-137. We show that this demand can be achieved if the braking index is small, $n \leq 2$ and the pulsar birth period is short, $P_b \simeq 1$ ms. Remarkably, this scenario can reproduce the size of HESS J1825-137 only in a dense environment with $n_{\text{ISM}} \geq 1 \text{ cm}^{-3}$. The requirement of the dense surrounding gas is supported by the presence of molecular clouds found in the source vicinity.

Keywords: Gamma rays: PWN - Radiation mechanisms: non-thermal

1. INTRODUCTION

Pulsar Wind Nebulae (PWNe) constitute a large non-thermal source population many representatives of which are prominent emitters of gamma-rays, especially in the Very High Energy (VHE; $E_\gamma \geq 100$ GeV) band (see, e.g., Kargaltsev et al. 2015, and references therein). These objects are formed in the course of the interaction of the pulsar wind with the surrounding matter – the interstellar medium (ISM) or the interior of the related Supernova Remnant (SNR). At this interaction, a substantial fraction of the pulsar’s spin-down energy is transferred to ultrarelativistic electrons with energies extending to 100 TeV and beyond. The subsequent interactions of these electrons with the ambient photon (basically, the Microwave Background Radiation; MBR) and magnetic fields result in the formation of synchrotron and inverse Compton (IC) nebulae in the X-ray and high energy gamma-ray bands. The energy losses of these electrons are shared between the synchrotron and IC radiation channels as $L_\gamma/L_X = w_{\text{MBR}}/w_B \approx 1(B/3\mu\text{G})^{-2}$. Thus, for most of PWNe with the magnetic field of order of 10 μG or less the gamma-ray production efficiency could exceed 10 %. Based on the assumption that the major fraction of the rotational energy of pulsars is released in ultrarelativistic electrons accelerated at the wind termination shock (TS), it has been predicted (Aharonian et al. 1997) that the ground based detectors with the performance typical for the current Atmospheric Cherenkov Telescopes should be able to reveal VHE gamma-ray component of radiation of tens of PWNe with spin-down luminosities $L \geq 10^{34}(d/1\text{ kpc})^2\text{ erg s}^{-1}$ (d is the distance to the source). The detection of almost 3 dozens of extended VHE gamma-ray sources in the vicinity of pulsars (see the TeVCAT catalog; <http://tevcat.uchicago.edu/>) in the indicated range of spin-down luminosities, supports this prediction. Thanks to the relatively large field of view, the good energy and angular resolutions, and the vast collection areas, the current gamma-ray telescopes¹ allow deep studies of energy-dependent morphologies of PWNe on angular scales of $\sim 1^\circ$. Moreover, the gamma rays being the product of inverse Compton scattering of electrons provide unambiguous model-independent information about the energy and spatial distribution of parent electrons. While the spectral energy distributions (SEDs) of X- and gamma rays from most of PWNe are comfortably described within the current models of PWNe, the reported TeV gamma-ray images extending

to $\sim 1^\circ$ do not have a simple explanation. For example, the angular size of HESS J1825–137, a PWN associated with the pulsar PSR J1826–1334, located at a distance of ~ 4 kpc, corresponds to the physical extension of the gamma-ray production region of 70 pc (Aharonian et al. 2006; Mitchell et al. 2017b,a). Indeed, the particle acceleration in PWNe is presumably linked to the pulsar wind termination, which in HESS J1825–137 is expected to occur at a relatively small distance from the pulsar, $R_{\text{TS}} < 0.1\text{ pc}$ (see, e.g., Van Etten & Romani 2011). The formation of such an extended TeV source requires either operation of a highly efficient particle transport or *in situ* particle (re)acceleration. There are two primary transport mechanisms for high-energy particles in PWNe: (i) advection by the macroscopic flow and (ii) diffusion. The characteristic propagation times depend strongly on the properties of the background plasma, which is determined, to a large extent, by the hydrodynamic flow. Thus, a consistent hydrodynamical description of PWNe is an essential element for understanding of the transport of relativistic particles in these objects. In this paper, we explore the formation of extended PWNe powered by a powerful pulsar in the context of hydrodynamics (HD) of the PWN-SNR system. The size of PWN determines the region where relativistic particles can advect with the nebular flow. As the zeroth order approximation, we ignore the dynamical impact of the magnetic field. The magnetic field in extended PWNe is typically small, but still, the magnetic pressure can be comparable to the particle pressure (see Van Etten & Romani 2011, for the case of HESS J1825–137). However, if one focuses on the expansion of a PWN, the main effect comes from the equation of state (EOS), which is typically taken as a polytropic with the index 4/3 for both the magnetized and non-magnetized relativistic plasma. The magnetic field can determine the preferred direction for the PWN expansion, as seen, for example, in the Crab Nebula. However, in the case of very extended PWNe, the non-homogeneity of ISM renders a much stronger influence on the PWN shape. The pure HD model can provide a simple, but still quite correct description for extended PWNe, without invoking the impact of the magnetic field.

2. A MODEL FOR PWN IN THE COMPOSITE SNR

SNRs that contain a PWN – the so-called composite SNRs – have a specific structure, which is presented schematically in Fig. 1. The part that is referred as PWN is filled with relativistic particles that originate from the pulsar. Bulk velocities in this region can be relativistic, in particular, close to its inner boundary,

¹ The potential of X-ray instruments in this regard are relatively modest

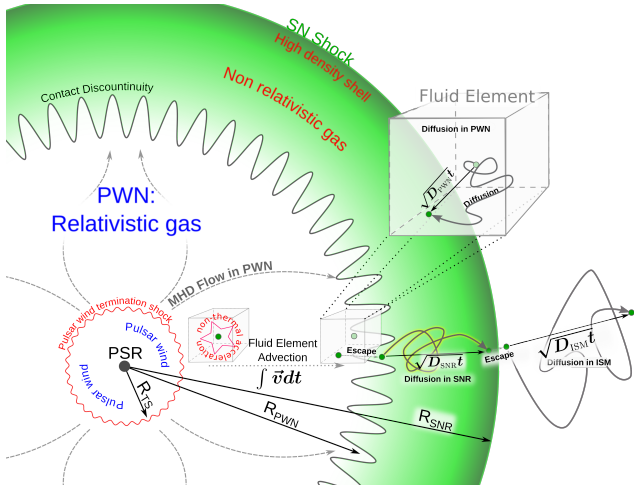


Figure 1. Schematic representation of the main zones and the particle transport mechanisms in composite SNR.

which is the pulsar wind termination shock. The contact discontinuity (CD) bounds the PWN from outside. The plasma velocities close to the CD are non-relativistic. Thus, an efficient advection in PWNe is most likely limited by the inner region of the nebula, which may, however, extend significantly beyond the termination shock. In contrast to advection, the diffusive transport is not constrained by any specific hydrodynamic region. It allows particles to escape from the PWN to the SNR region. Apparently, the diffusion coefficients in PWN and SNR may differ significantly. Similarly, the advection in the SNR is limited by the region between the CD and the SN shock. In this region, the flow velocities are small ($\sim 10^4 \text{ km s}^{-1}$). The diffusion in the SNR leads to the particle escape. The high energy particles from the SNR can penetrate PWN or eventually escape to ISM. In the ISM, the diffusion proceeds at a rate corresponding to the diffusion of the galactic Cosmic Rays (CRs). Note that in the Galactic Disk the CR diffusion is much (orders of magnitude) faster compared to the diffusion in the Bohm limit. Finally, advection in ISM might be relevant only in the case of high proper velocity of the pulsar. The evolution and the structure of PWNe are essential for understanding of the origin of radiation seen from these objects. The study of various aspect of PWN has a long history. Pacini & Salvati (1973a) studied the evolution of the magnetic field at the early epoch of formation of the Crab Nebula and explored the impact of this evolution on the distribution of non-thermal particles and strength of the magnetic field at the present epoch (Pacini & Salvati 1973b). The impact of the dynamics of PWN on a self-gravitating shell was investigated by Maceroni et al. (1974). Later on, Reynolds & Chevalier (1984) proposed a comprehensive

model describing the dynamics of evolution of the PWN in the SNR (see also Bucciantini et al. 2011). In some other studies, the structure of PWN within a slowly expanding SNR shell has been explored (Rees & Gunn 1974). This approach has been developed into a detailed 1D magnetohydrodynamic (MHD) model for the Crab Nebula (Kennel & Coroniti 1984a,b). The latter describes remarkably well the broad-band SED of the Crab Nebula from the optical to soft gamma-ray band through the synchrotron radiation and in the VHE band through the IC scattering of electrons (Atoyan & Aharonian 1996). Finally, in recent years different aspects of the PWN evolution have been addressed through 2D and 3D (M)HD numerical simulations. In particular, a significant progress has been achieved in the modeling of X-ray morphology caused by the pulsar wind anisotropy (see, e.g., Del Zanna et al. 2004; Porth et al. 2014) and by the reverse shock at the later stages of evolution of the PWN (Kolb et al. 2017). In this paper, we develop an analytical model to describe the dynamics of evolution of the anomalously extended PWNe. Generally, the studies of PWN silently assume that the dominant contribution to the energy of a composite SNR is provided by the supernovae (SN) explosion. Indeed, the total deposited energy by one of the currently most powerful pulsars, the Crab pulsar, is estimated as $3 \times 10^{50} \text{ erg}$, which is significantly smaller than the energy transferred to the ejecta at the SN Type II explosion (Reynolds & Chevalier 1984). If the SNR energy is dominated by the SN explosion, then the Sedov's solution provides a rather accurate estimate of the source size. In this case, extended PWNe, with a size of $\gtrsim 10 \text{ pc}$, are possible only in regions characterized by extremely low density of interstellar medium (e.g. de Jager & Djannati-Ataï 2009). The required density, as low as $n \approx 10^{-3} \text{ cm}^{-3}$, is not typical for the conventional regions of the interstellar medium in the Galactic Plane. Moreover, in the specific case of HESS J1825–137, it is not supported by observations which revealed dense molecular clouds in the vicinity of HESS J1825–137 (Voisin et al. 2016). Below we explore whether the problem can be resolved (or at least relaxed) in the case of injection of a large amount of energy by the pulsar that dominates over the SN explosion energy. In this case, the dynamics of the system should be similar to the *Phase IV* of the scheme discussed by Reynolds & Chevalier (1984). However, it is important to explicitly account for the dynamics of the interstellar medium involved into the motion. Indeed, the mass of interstellar matter located in a region with a radius $R_{\text{SNR}} = 10 \text{ pc}$ can achieve $100 M_{\odot}$ for the mean proton density of 1 cm^{-3} . We propose a dynamic model that accounts for these two important factors, the

dominant pulsar contribution to the dynamics of SNR and the inertia of the interstellar medium.

2.1. The contribution of pulsar to the overall SN energy

The pulsar rotation losses are determined through the time dependence of its angular velocity:

$$\dot{E} = I\Omega\dot{\Omega}, \quad (1)$$

where Ω , $\dot{\Omega}$, and I are the pulsar angular velocity, its time derivative, and the moment of inertia of the neutron star (NS), respectively. The later is calculated using the relation:

$$I = \frac{2}{5} R_{\text{PSR}}^2 M_{\text{PSR}} \simeq 10^{45} \text{ g cm}^2 \left[\left(\frac{M_{\text{PSR}}}{1.4 M_{\odot}} \right) \left(\frac{R_{\text{PSR}}}{10 \text{ km}} \right)^2 \right]. \quad (2)$$

It is conventionally assumed that the change of the angular velocity is determined by the braking index, n :

$$\dot{\Omega} \propto \Omega^n. \quad (3)$$

If the time $t' = 0$ corresponds to the present epoch, the pulsar parameters evolve with time as

$$\Omega = \frac{\Omega_p}{(1 + t'/t'_0)^{\frac{1}{n-1}}}, \quad (4)$$

$$\dot{\Omega} = \frac{\dot{\Omega}_p}{(1 + t'/t'_0)^{\frac{n}{n-1}}}, \quad (5)$$

and

$$L_{\text{sd}}(t) = \frac{L_p}{(1 + t'/t'_0)^{\frac{n+1}{n-1}}}. \quad (6)$$

Here, Ω_p and $\dot{\Omega}_p$ are the current angular velocity and the angular acceleration, respectively. The characteristic time, t'_0 is determined by the pulsar *characteristic* age, $\tau = -\Omega_p/2\dot{\Omega}_p$, and the braking index:

$$t'_0 = \frac{2\tau}{(n-1)}. \quad (7)$$

In the above treatment the pulsar birth epoch, $-t'_0 < t'_b < 0$, is uncertain. For almost all pulsars, the measured values of the braking index, n , vary between 1 and 3 (Lyne et al. 1993; Boyd et al. 1995; Lyne et al. 1996; Livingstone et al. 2007; Weltevredre et al. 2011; Livingstone et al. 2011; Roy et al. 2012), with two exceptions: PSR J1734–3333 ($n = 0.9 \pm 0.2$, Espinoza et al. 2011) and PSR J1640–4631 ($n = 3.15 \pm 0.03$, Archibald et al. 2016). Thus, the true age of the pulsar can exceed, by a factor > 5 , the characteristic age, τ (see, e.g., de Jager

et al. 2005). The birth angular velocity is constrained by the centrifugal breakup limit:

$$\Omega < \Omega_{\text{br}} = \sqrt{\frac{GM_{\text{PSR}}}{R_{\text{PSR}}^3}} = \Omega_{\text{br}}^{(0)} \left[\left(\frac{M_{\text{PSR}}}{1.4 M_{\odot}} \right)^{1/2} \left(\frac{R_{\text{PSR}}}{10 \text{ km}} \right)^{-3/2} \right], \quad (8)$$

where $\Omega_{\text{br}}^{(0)} = 1.4 \times 10^4 \text{ s}^{-1}$ corresponds to the breakup velocity for the conventional size of the NS. This allows us to constrain the birth epoch:

$$\frac{t'_b}{t'_0} > \left(\frac{\Omega_p}{\Omega_{\text{br}}} \right)^{n-1} - 1. \quad (9)$$

The breakup angular velocity, $\Omega_{\text{br}}^{(0)}$, corresponds to the sub-millisecond period $P_{\text{br}}^{(0)} \simeq 0.5 \text{ ms}$, thus for the typical pulsar periods, $\Omega_p/\Omega_{\text{br}} \ll 1$, the correction is small. This constraint, however, implies a limit on the birth spin-down luminosity:

$$L_b < L_{\text{br}} = L_p \left(\frac{\Omega_{\text{br}}}{\Omega_p} \right)^{n+1}. \quad (10)$$

The entire energy released by the pulsar since its birth at t_b is

$$E = \int_{t'_b}^0 dt' L_{\text{sd}}(t') = L_p \tau \left(\left(\frac{\Omega_b}{\Omega_p} \right)^2 - 1 \right) = \frac{I (\Omega_b^2 - \Omega_p^2)}{2}, \quad (11)$$

where Ω_b is the birth angular velocity. Unless, the mass and the size of the NS strongly deviate from their conventional values, the breakup constraint limits the total energy released by the pulsar:

$$E < L_p \tau \left(\frac{\Omega_{\text{br}}}{\Omega_p} \right)^2 = \frac{I \Omega_{\text{br}}^2}{2} \sim 10^{53} \text{ erg s}^{-1} \left[\left(\frac{M_{\text{PSR}}}{1.4 M_{\odot}} \right)^2 \left(\frac{R_{\text{PSR}}}{10 \text{ km}} \right)^{-1} \right]. \quad (12)$$

Note that E does not depend on the pulsar braking index n . This estimate ignores, however, the effects related to the dependence of the moment of inertia on pulsar's angular velocity. For example, for the velocities close to the breakup limit, the shape of the NS should deviate significantly from the spherical one, resulting in the dependence of I on Ω (see, e.g., Hamil et al. 2015). The evolution of the NS magnetic field and direction of the magnetic momentum can also lead to

a non-trivial dependence of the braking index on time (see, e.g., [Hamil et al. 2016](#); [Rogers & Safi-Harb 2016, 2017](#)). The consideration of these effects is beyond the scope of this paper. The angular velocity of a pulsar at its birth cannot be very close to the breakup limit. Indeed, since in this case the pulsar is not gravitationally bound, no energy would be available for the SN explosion. The rotation energy should be small compared to the NS gravitational bound energy. The bulk of the gravitational energy released during the formation of the compact object is expected to escape with the neutrino emission, and only a tiny fraction, $\sim 1\%$, is transferred to the ejecta, $E_{\text{ej}} \sim 10^{51} \text{erg}$. Thus, the pulsar rotation energy at its birth could be small compared to the breaking limit, but still can exceed the initial kinetic energy of the SN shell. In this case, the dimensions of the SNR and the PWN are determined by the pulsar injection energy.

2.2. Structure of the Composite SNR

The expansion of the PWN determines the evolution of distribution of non-thermal particles and the strength of the magnetic field. Given the relativistic nature of plasma in PWN, at the stages relevant for the modeling of the present-day non-thermal emission, the hydrodynamic processes in the PWN should proceed in the nearly adiabatic regime. Thus, the internal structure of the nebula can be described analytically. On the other hand, the state of the non-relativistic shell may depend strongly on its dynamics at earlier stages of the expansion. To explore this evolution, we use a simple dynamic model. The energy of the system is distributed between three components: the kinetic energy of the shell (SNR shell), the internal energy of the non-relativistic gas in the shell, and the internal energy of the relativistic gas in the nebula. The SNR shell occupies the region between the external boundary of the PWN at R_{PWN} , and the SNR radius, R_{SNR} . The mass of the SNR shell is determined by the gas density of ISM, ρ_{ISM} , and the shell radius. The SNR density varies strongly throughout the shell: the mass is concentrated in a thin layer at R_{SNR} , while the hot non-relativistic gas fills the remaining part of the shell. The pressure in the hot part of the shell, P , equals to the pressure of the relativistic gas in the PWN. To describe the system, we use a model that includes the following relations:

1. the equation for the energy balance in the nebula:

$$3 \frac{dPV_{\text{PWN}}}{dt} + P \frac{dV_{\text{PWN}}}{dt} = L_{\text{sd}}(t); \quad (13)$$

2. the equation for the energy balance in the non-relativistic shell:

$$\frac{d}{dt} \left(\frac{Mv^2}{2} + \frac{3}{2} P (V_{\text{SNR}} - V_{\text{PWN}}) \right) = P \frac{dV_{\text{PWN}}}{dt}, \quad (14)$$

where v is the shell velocity;

3. the equation of motion:

$$\frac{dMv}{dt} = 4\pi R_{\text{SNR}}^2 P. \quad (15)$$

Let t be the time since the pulsar's birth:

$$t = t' - t'_b, \quad (16)$$

where the birth epoch is

$$t'_b = -t'_0 \left[1 - \left(\frac{\omega}{\tilde{\omega}} \right)^{n-1} \right]. \quad (17)$$

Here we express the pulsar's current angular velocity and the velocity at the birth, as fractions of the breakup velocity: $\Omega_p = \omega \Omega_{\text{br}}^{(0)}$ and $\Omega_b = \tilde{\omega} \Omega_{\text{br}}^{(0)}$, respectively. The pulsar's time-dependent spin-down luminosity is

$$L_{\text{sd}}(t) = \frac{L_p (\tilde{\omega}/\omega)^{(n+1)}}{(1 + t/t_0)^{\frac{n+1}{n-1}}}, \quad (18)$$

where the characteristic slow-down time is

$$t_0 = \frac{2\tau}{(n-1)} \left(\frac{\omega}{\tilde{\omega}} \right)^{n-1}. \quad (19)$$

Obviously, the present epoch corresponds to $t_p = -t'_b$.

2.2.1. Asymptotic Expansion

For $t \gg t_0$, the pulsar injection ceases significantly, and the expansion of the SNR is dominated by the initial energy release. At the initial stage of evolution of the PWN inside of the composite SNR does not proceed adiabatically because of the energy injection by the pulsar (see, e.g., [Reynolds & Chevalier 1984](#)) and the severe radiative losses caused by the strong magnetic field ([Pacini & Salvati 1973a](#)). However, timescales exceeding the pulsar slowdown time, the intensity of the injection by the pulsar ceases. The extension of the nebula results in the reduction of the magnetic field and suppression of radiative losses. Thus, at the later stages of expansion, the PWN should evolve adiabatically. The approach suggested by [Zel'dovich & Raizer \(1967\)](#) can be generalized to describe the evolution of the PWN. The energy of the system consisting of a PWN and the SNR shell is

$$E = \frac{4\pi}{3} \left(\frac{\rho_{\text{ISM}} \dot{R}_{\text{SNR}}^2}{2} R_{\text{SNR}}^3 + \frac{3P}{2} (R_{\text{SNR}}^3 - R_{\text{PWN}}^3) + 3PR_{\text{PWN}}^3 \right), \quad (20)$$

where the first and second terms describe the contribution from the shell, and the third term characterises the contribution from PWN. At later stages, the main contribution to the change of the kinetic energy of the shell is due to the increase of its mass, thus

$$P \propto \rho_{\text{ISM}} \dot{R}_{\text{SNR}}^2. \quad (21)$$

This allows us to express the energy of the system as

$$E = 2\pi P (R_{\text{PWN}}^3 + k R_{\text{SNR}}^3), \quad (22)$$

where k is a dimensionless constant. Since the expansion is adiabatic, $PR_{\text{PWN}}^4 = \text{const.}$ E and P are related as

$$2\pi P R_{\text{PWN}}^4 = aE \quad (23)$$

or equivalently

$$\dot{R}_{\text{SNR}}^2 \propto a \frac{E}{\rho_{\text{ISM}}} R_{\text{PWN}}^{-4}. \quad (24)$$

Here a is a constant of length dimension. The expression for the energy can be simplified as

$$R_{\text{PWN}}^3 (R_{\text{PWN}} - a) = ka R_{\text{SNR}}^3. \quad (25)$$

Combining the above two equations, one obtains

$$\dot{R}_{\text{PWN}} \propto a^{5/6} \sqrt{\frac{E}{\rho_{\text{ISM}}}} \frac{(R_{\text{PWN}} - a)^{2/3}}{R_{\text{PWN}} (R_{\text{PWN}} - 3a/4)}. \quad (26)$$

This equation has an analytic solution, which in the asymptotic limit $R_{\text{PWN}} \gg a$ is reduced to

$$R_{\text{PWN}} \propto a^{1/4} \left(\frac{Et^2}{\rho_{\text{ISM}}} \right)^{3/20}. \quad (27)$$

The radius of the PWN allows us to determine the shell radius and the pressure of the SNR (see Eqs. (24) and (21)):

$$R_{\text{SNR}} \propto \left(\frac{Et^2}{\rho_{\text{ISM}}} \right)^{1/5} \quad (28)$$

and

$$P \propto \rho_{\text{ISM}} \left(\frac{E}{\rho_{\text{ISM}} t^3} \right)^{2/5}. \quad (29)$$

Finally, the ratio of the pulsar spindown luminosity and the pressure determines the location of the pulsar wind termination shock:

$$R_{\text{TS}} \propto \sqrt{\frac{L(t)}{P}} \propto t^{\frac{3}{5} - \frac{n+1}{2(n-1)}}. \quad (30)$$

Although the SNR expansion is similar to the Sedov's solution (although with a different numerical coefficient), the PWN expands slower with time: $R_{\text{PWN}} \propto t^{0.3}$. To infer the details of the SNR expansion, we solve the system of dynamic equations numerically.

2.2.2. Numerical Model

The dynamic equations can be completed with the following phenomenological relations for the shell momentum

$$Mv = \frac{4\pi}{3} R_{\text{SNR}}^3 C_m \rho_{\text{ISM}} \frac{dR_{\text{SNR}}}{dt}, \quad (31)$$

and the shell kinetic energy

$$\frac{Mv^2}{2} = \frac{4\pi}{3} R_{\text{SNR}}^3 C_e \rho_{\text{ISM}} \left(\frac{dR_{\text{SNR}}}{dt} \right)^2. \quad (32)$$

Adjusting the constants C_m and C_e provides a better agreement between the prediction of this simple model and the more accurate numerical treatment. In the case of a strong explosion in a medium with adiabatic index $5/3$, the blast wave radius and pressure are

$$R_{\text{SNR}} = \left(\frac{\alpha E t^2}{\rho_{\text{ISM}}} \right)^{1/5} \quad (33)$$

and

$$P = \beta P_{\text{SNR}} = \frac{3\beta}{4} \rho_{\text{ISM}} \left(\frac{dR_{\text{SNR}}}{dt} \right)^2, \quad (34)$$

where $\alpha \simeq 1.29$ and $\beta = 0.3$ are dimensionless coefficients. The solution of the system correctly reproduces the blast wave radius and the pressure if one adopts $C_m = \frac{3\beta}{2} \approx 0.45$ and $C_e = \frac{75}{16\pi\alpha} - \frac{9\beta}{8} \approx 0.82$ (see Appendix A for the details). The system of dynamic equations and phenomenological relations can be reduced to the following system:

$$\frac{dP}{dt} = \rho_{\text{ISM}} \frac{5x^2 A - 8B}{(4 + x^3) R_{\text{SNR}}}, \quad (35)$$

$$\frac{dR_{\text{PWN}}}{dt} = \rho_{\text{ISM}} \frac{(1 - x^3) A + 2xB}{(4 + x^3) P}, \quad (36)$$

$$\frac{dV_{\text{SNR}}}{dt} = \frac{3 \frac{P}{\rho_{\text{ISM}}} - 3C_m V_{\text{SNR}}^2}{C_m R_{\text{SNR}}}, \quad (37)$$

$$\frac{dR_{\text{SNR}}}{dt} = V_{\text{SNR}}. \quad (38)$$

Here the following notations are used:

$$x = \frac{R_{\text{PWN}}}{R_{\text{SNR}}}, \quad A = \frac{L}{4\pi \rho_{\text{ISM}} R_{\text{PWN}}^2}, \quad (39)$$

and

$$B = V_{\text{SNR}} \left[\left(\frac{2C_e}{C_m} + \frac{3}{2} \right) \frac{P}{\rho_{\text{ISM}}} - 3C_e V_{\text{SNR}}^2 \right]. \quad (40)$$

Similarly to the Sedov's solution, the inertia of the ISM affects the expansion of the SNR through the dimensionless parameter,

$$s = \sqrt{\frac{L_0 t_0^3}{\rho_{\text{ISM}} R_0^5}}, \quad (41)$$

where R_0 , t_0 , and L_0 are the characteristic spatial-, time- and energy- scales (see Appendix B for the dimensionless form of equations).

2.2.3. Initial Conditions

Equations (35) – (38) can be solved numerically, e.g., using the Runge-Kutta method. To proceed with the integration, one needs to define the initial values for P , R_{PWN} , R_{SNR} , and V_{SNR} . The initial values related to the SNR shell should account for the energy transferred at the SN explosion to the ejecta

$$\left. \frac{4\pi}{3} \rho_{\text{ISM}} R_{\text{SNR}}^3 V_{\text{SNR}}^2 \right|_{t=0} \simeq E_{\text{EJ}}. \quad (42)$$

The initial radii of the PWN and SNR should satisfy the obvious condition $R_{\text{PWN}} < R_{\text{SNR}} \ll 1$ pc. Also, the initial energy of the relativistic gas should be small compared to the characteristic energy injected by the pulsar:

$$\left. \frac{4\pi}{3} \rho_{\text{ISM}} R_{\text{PWN}}^3 P \right|_{t=0} \ll L_b t_0. \quad (43)$$

If these requirements are satisfied, the impact of the initial conditions on the solution of Eqs. (35) – (38) is weak and vanishes once the energy injected by the pulsar significantly exceeds the initial energy. The pulsar initial condition is determined by its birth angular velocity, or, equivalently, by its birth epoch for the given braking index; see Eqs. (17) – (19). A typical solution of the system Eqs. (35) – (38) is shown in Fig. 2.

3. IMPLICATIONS FOR HESS J1825–137

3.1. Size of the nebula

For the estimated distance to the source of HESS J1825–137 of 4 kpc, the $\approx 1^\circ$ angular size of the latter corresponds to 70 pc linear size of the gamma-ray production region. Although the gamma-ray image deviates from the spherically symmetric shape, below for simplicity we will assume that the radius of the source is 35 pc. The detection of a H α rim at a distance of 120 pc from the pulsar PSR J1826-1334 has been interpreted as a signature of the progenitor SNR (see Stupar et al. 2008; Voisin et al. 2016). If the kinetic energy of the ejecta provides the main contribution to the energy budget, then the anisotropic extension of the SNR is determined by the density of the external environment.

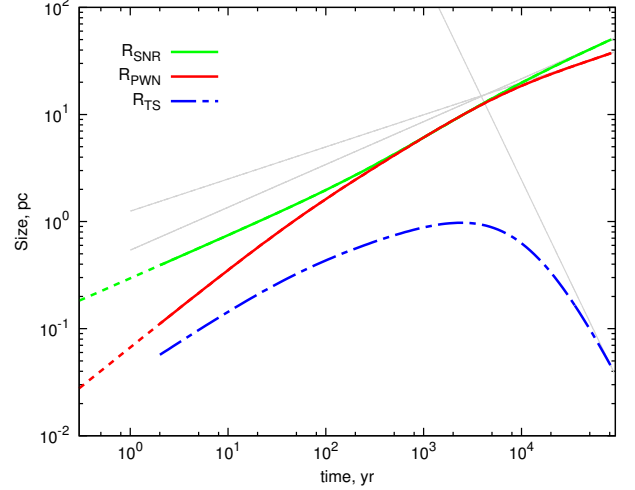


Figure 2. Numerical solution of the system Eqs. (35) – (38) together with lines showing the asymptotic behavior as predicted by Eqs. (28), (27), and (30). The pulsar angular velocity and the braking index are assumed to be $\tilde{\omega} = 0.5$ and $n = 1.5$, respectively. The calculation is performed for ISM with mean gas number density $\bar{n}_{\text{ISM}} = 1 \text{ cm}^{-3}$.

The Sedov's solution gives a reliable estimate for the SNR radius:

$$\begin{aligned} R_{\text{SNR}} &\simeq \left(\frac{1.3 E_{\text{EJ}} t_p^2}{\rho_{\text{ISM}}} \right)^{1/5} \\ &\sim 12 \left(\frac{E_{\text{EJ}}}{10^{51} \text{ erg}} \right)^{1/5} \left(\frac{t_p}{10 \text{ kyr}} \right)^{2/5} \left(\frac{\bar{n}_{\text{ISM}}}{1 \text{ cm}^{-3}} \right)^{-1/5} \text{ pc}, \end{aligned} \quad (44)$$

where $\rho_{\text{ISM}} = \bar{n}_{\text{ISM}} m_p$ are the density, the hydrogen number density, and the proton mass, respectively. If the expansion is super-sonic, there should not be effective communications between different parts of the shock. Therefore, the distance from the explosion point to the SNR shell is determined by the average gas density in the corresponding direction, $\bar{\rho}_{\text{ISM}}$. Thus, the SNR shell can be located at the distance of ~ 120 pc, as if

$$\left(\frac{t_p}{10 \text{ kyr}} \right)^2 \left(\frac{E_{\text{EJ}}}{10^{51} \text{ erg}} \right) \left(\frac{\bar{n}_{\text{ISM}}}{1 \text{ cm}^{-3}} \right)^{-1} \sim 10^5. \quad (45)$$

The ejecta energy at SN type II is constrained by $E_{\text{EJ}} \simeq 3 \times 10^{51} \text{ erg s}^{-1}$, while the age of the source is limited by $t_p < 100 \text{ kyr}$ (for $n = 1.4$). Thus, the Sedov's solution is consistent with the observed size of the SNR only if $\bar{n}_{\text{ISM}} < 10^{-2} \text{ cm}^{-3}$. Note that de Jager & Djannati-Ataï (2009) derived somewhat smaller (by a factor of 3) upper limit for \bar{n}_{ISM} assuming for the braking index $n = 2$. This upper limit is substantially below the typical density of the interstellar gas in the Galactic Plane. Moreover, Voisin et al. (2016) reported the presence of several molecular clouds in the small angular

proximity to the nebula with an average number density $n_c \sim 10^3 \text{ cm}^{-3}$ and characteristic size $r_c \sim 10 \text{ pc}$. It is likely that one of these clouds is responsible for the anisotropic expansion of the nebula, thus it should be located close to the nebula. The gas density in molecular clouds is expected to follow the King's profile:

$$\rho = \frac{\rho_c}{(1 + r/r_c)^2}. \quad (46)$$

Thus, the density to the south of the pulsar can hardly be as low as it is required by the Sedov's solution. Instead, it should be comparable to the upper limit of $n_{\text{ISM}} \sim 4 \text{ cm}^{-3}$ obtained by [Voisin et al. \(2016\)](#). To avoid this problem, we suggest an alternative scenario in which the energy injection by the pulsar dominates over the kinetic energy of the ejecta. This scenario has two advantages: (i) it offers significantly larger available energy, (ii) because of the high sound velocity in the PWN, the energy is predominately used for the expansion in the directions of the lower density. Thus, the position of the SNR shell and the size of the PWN can provide decisive inspection for the suggested scenario. The energy for the source expansion is transferred through the PWN, which evolves adiabatically. The energy consumed for the expansion is determined by the volumes of the PWN and SNR. Thus, their sizes should be measured neither from the SN explosion point nor from the present pulsar location. Instead one should use, as a starting point, the geometrical center of the current structure. This allows us to translate the H.E.S.S. and optical observations to the following requirements to be met by the 1D model: Below we adopt the following requirements to be met by the 1D model: $R_{\text{TS}} \sim 0.03 \text{ pc}$, $R_{\text{PWN}} \sim 35 \text{ pc}$, and $R_{\text{SNR}} \sim 50 \text{ pc}$. For the present-day spin-down luminosity and the characteristic age of the pulsare, the size of the the composite SNR is determined by three parameters: braking index n , the initial rotation velocity $\tilde{\omega}$, and the density of the surrounding medium $\bar{\rho}_{\text{ISM}}$. The results of calculation of the present-day size are shown in Figs. 3 and 4. These calculations allow determination of the numerical coefficients for the asymptotic expressions given by Eqs. (28) and (30):

$$R_{\text{SNR}} \simeq 52 \left(\frac{\tilde{\omega}^2}{(n-1)^2 \rho_0} \right)^{1/5} \text{ pc}, \quad (47)$$

$$R_{\text{TS}} \simeq 0.028 ((n-1)^6 \tilde{\omega}^4 \rho_0^3)^{-1/10} \text{ pc}, \quad (48)$$

where $\rho_0 = \bar{\rho}_{\text{ISM}}/(m_p \text{ cm}^{-3})$. For $\tilde{\omega} > 0.1$ and $n > 1.5$, these approximation are rather accurate; it can be checked from the comparison of the results of numerical calculations shown in Figs. 3 and 4. For small values of $\tilde{\omega} \leq 0.1$, the pulsar contribution to the overall energy

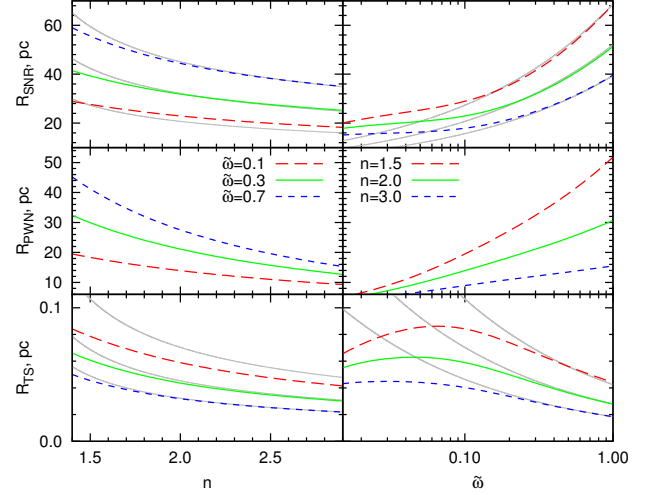


Figure 3. Present-day radii of the SNR (top panels), PWN (middle panels), and pulsar wind termination shock (bottom panels) as functions of the pulsar braking index n (left panels) and pulsar birth angular velocity (right panels). In the left panels, the calculations are performed for three values of the pulsar angular velocity at its birth: $\tilde{\omega} = 0.1, 0.3$, and 0.7 . These numbers correspond to 1%, 10%, and 50% of the pulsar gravitational energy. In the right panels the calculations are performed for three values of the braking index $n = 1.5, 2$, and 3 . The adopted number density of the surrounding gas is $\bar{n}_{\text{ISM}} = 1 \text{ cm}^{-3}$. The thin grey lines show analytic approximations given by Eqs. (47) and (48).

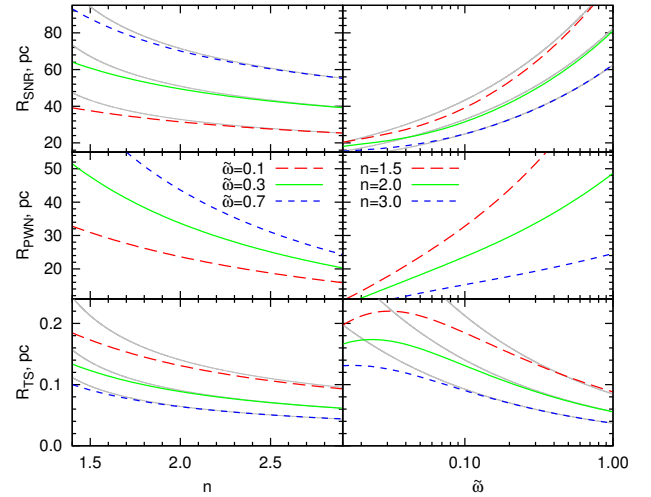


Figure 4. The same as in Fig. 4 but for $\bar{n}_{\text{ISM}} = 0.1 \text{ cm}^{-3}$.

budget becomes comparable to the assumed initial energy of the SNR shell, which was ignored when deriving these expressions. Also, it is assumed that the bulk of the pulsar rotation energy is promptly released at the initial phase. This assumption violates for small values of the braking index n . Finally, we note that because of presence of parameter a in Eq. (27), the size of the PWN

cannot be described by an approximate formula similar to Eqs. (47) and (48). A comparison of Eq. (48) with the termination shock radius implies that the density of the medium should be rather high, $\bar{n}_{\text{ISM}} \sim 1 \text{ cm}^{-3}$. For this high medium density, the SNR and PWN can be sufficiently extended if $\tilde{\omega} > 0.5$ and $n \leq 2$ as shown in Fig. 3.

4. SUMMARY

The total energy released at a SN type II explosion, 10^{53} erg , exceeds, by two orders of magnitude, the energy transferred to the ejecta, $E_{\text{EJ}} \sim 10^{51} \text{ erg}$. The bulk of energy escapes with the neutrino emission. Typically, the pulsar rotation energy is small compared to the ejecta energy. However, it cannot be excluded that at some circumstances the pulsar can obtain a larger fraction of the explosion energy. If it becomes comparable to the kinetic energy of the ejecta, the sizes of the SNR and PWN can significantly deviate from the Sedov's solution resulting in formation of extended nebulae and PWNe. To illustrate the implication of this scenario, we considered a specific case of HESS J1825–137, a very extended and bright in VHE gamma rays PWN (Aharonian et al. 2006; Mitchell et al. 2017b,a). The X-ray and gamma-ray observations of HESS J1825–137 show that the shape of the nebula deviates from the spherically symmetric geometry. Thus, the 1D model described in Sec. 2 has a limited capability for accurate quantitative predictions. However, in the framework of the suggested scenario, the hydrodynamic processes evolve differently from the conventional situations, and the 1D model should provide a correct estimate for the energy required for the PWN/SNR inflation. In the frameworks of the scenario, the pressure in the PWN is the main driving force of the SNR expansion. Independently on symmetry of the system and dimension of the used model, the PWN is nearly isobaric; thus the radius of the pulsar wind termination shock provides an observational constraint for the pressure in the nebula. Therefore, we adopt the following requirement: the present day pressure in the nebula should be consistent with the pulsar wind termination shock located at $R_{\text{TS}} \sim 0.03 \text{ pc}$ from the pulsar (Van Etten & Romani 2011). The 1D model allows us to obtain the radii of the SNR, PWN, and pulsar wind termination shock as functions of three key model parameters: density of the ISM, pulsar braking index, and the initial

angular velocity of the pulsar. In the framework of this model, it is possible to reproduce the three key properties of the system: $R_{\text{SNR}} \geq 50 \text{ pc}$, $R_{\text{PWN}} \geq 35 \text{ pc}$, and $R_{\text{TS}} \simeq 0.03 \text{ pc}$, provided that (i) the pulsar obtains, at its birth, more than 25% of the explosion energy ($\tilde{\omega} \geq 0.5$), and (ii) the braking index is small, $n \leq 2$. In contrast to the conventional Sedov-like solution that implies an extremely (almost unrealistically) low density of the ISM, $\bar{n}_{\text{ISM}} < 10^{-2} \text{ cm}^{-3}$, the proposed model requires a rather dense environment in the ISM, $\bar{n}_{\text{ISM}} \sim 1 \text{ cm}^{-3}$. To a certain extent, this requirement is supported by the presence of dense molecular clouds reported in the vicinity of the source (Voisin et al. 2016). What concerns the requirement for the pulsar braking index, $n \leq 2$, it is small compared to the value measured for the Crab pulsar (Lyne et al. 1993). But it seems to be reasonable for both the old (e.g., Vela; $n = 1.4 \pm 0.2$, Lyne et al. 1996) and young (e.g., J1833–1034; $n = 1.8569 \pm 0.001$, Roy et al. 2012) pulsars. The most demanding requirement for the suggested scenario is the initial rotation energy of the pulsar. Our simulations require fast angular velocity at the birth, $\tilde{\omega} \geq 0.5$, which implies very small initial rotation period, $P_{\text{b}} \leq 1 \text{ ms}$. This translates to a lower limit on the birth spin-down luminosity:

$$L_{\text{b}} > 3 \times 10^{41} \text{ erg s}^{-1}, \quad (49)$$

for the braking index and the initial angular velocity: $n = 1.5$ and $\tilde{\omega} = 0.5$, respectively. The requirement for the very fast initial rotation may seem an extreme assumption. However, as Heger et al. (2005) have shown, the differential rotation in a massive progenitor should result in formation of a rapidly rotating pulsar. For example, numerical simulations predict birth of a pulsar with $P_{\text{b}} = 3 \text{ ms}$ for a $35 M_{\odot}$ progenitor star. Thus, the option of an initially very fast rotating pulsar *a priori* cannot be excluded. It should be considered along with the conventional scenario that provides an explanation of the very large size of HESS J1825–137 assuming an extremely low density environment surrounding the source.

The work of F. Aharonian, S.V. Bogovalov, and G.V. Ustuygova was supported by the Russian Science Foundation, project no. 16-12-10443.

APPENDIX

A. NUMERICAL MODEL FOR SN EXPLOSION

If the injection of energy by the PWN is sufficiently small to have an impact on the dynamics of the SNR, the dynamic equations consist of the requirement of the *energy conservation*:

$$\frac{d}{dt} \left(\frac{Mv^2}{2} + \frac{3PV_{\text{SNR}}}{2} \right) = 0 \ ; \quad (\text{A1})$$

and the *Second Newton's law* :

$$\frac{dMv}{dt} = 4\pi R_{\text{SNR}}^2 P \ . \quad (\text{A2})$$

Here it is adopted that the shell mass is concentrated close to the blast wave. Eqs. (A1) and (A2) can be completed with empirical relations for the shell's momentum and kinetic energy:

$$Mv = C_m \rho_{\text{ISM}} \frac{4\pi R_{\text{SNR}}^3}{3} \frac{dR_{\text{SNR}}}{dt}, \quad \frac{Mv^2}{2} = C_e \rho_{\text{ISM}} \frac{4\pi R_{\text{SNR}}^3}{3} \left(\frac{dR_{\text{SNR}}}{dt} \right)^2 \ .$$

The solution of the hydrodynamics equation allows us to find numerically the coefficients for the Sedov's self-similar solution. Namely, the blast wave radius, R_{SNR} , and pressure at explosion point, P_c , are

$$R_{\text{SNR}} = \left(\frac{\alpha E t^2}{\rho_{\text{ISM}}} \right)^{1/5}, \quad P = \beta P_c = \frac{3\beta}{4} \rho_{\text{ISM}} \dot{R}_{\text{SNR}}^2 \ ,$$

where E and P are the explosion energy and pressure behind the blast wave. For politropic gas with $\gamma = 5/3$, the numerical coefficients are $\alpha \approx 1.29$, $\beta \approx 0.3$. Eq. (A1) can be integrated yielding in

$$\frac{Mv^2}{2} + \frac{3PV}{2} = \frac{4\pi}{3} \rho_{\text{ISM}} C_e R_{\text{SNR}}^3 \dot{R}_{\text{SNR}}^2 + \frac{4\pi}{3} R_{\text{SNR}}^3 \frac{3P}{2} = \frac{4\pi}{3} R_{\text{SNR}}^3 \left(\rho_{\text{ISM}} C_e \dot{R}_{\text{SNR}}^2 + \frac{3P}{2} \right) = E \ . \quad (\text{A3})$$

In turn, Eq. (A3) is fulfilled if

$$\dot{R}_{\text{SNR}} = A R_{\text{SNR}}^{-3/2} \ , \quad (\text{A4})$$

$$P = B R_{\text{SNR}}^{-3} \ . \quad (\text{A5})$$

Note that

$$\frac{4\pi}{3} \left(\rho_{\text{ISM}} C_e A^2 + \frac{3B}{2} \right) = E \ . \quad (\text{A6})$$

Solving Eq. (A4) one obtains $R_{\text{SNR}} = \left(\frac{5At}{2} \right)^{2/5} = \left(\frac{\alpha E t^2}{\rho_{\text{ISM}}} \right)^{1/5}$, $\frac{25A^2}{4} = \frac{\alpha E}{\rho_{\text{ISM}}}$, which yields in $A^2 = \frac{4\alpha E}{25\rho_{\text{ISM}}}$.

Changing variables in Eq. (A2) as R_{SNR} , $dR_{\text{SNR}} = Ddt$, $D = \dot{R}_{\text{SNR}}$, one obtains

$$\frac{4\pi}{3} \rho_{\text{ISM}} C_m \frac{dR_{\text{SNR}}^3 D}{dR_{\text{SNR}}} = 4\pi \frac{R_{\text{SNR}}^2 P}{D} \ . \quad (\text{A7})$$

Substituting in Eq. (A7) one derives that $\frac{\rho_{\text{ISM}} C_m A^2}{2} = B$. Thus, the following chain of equations should be satisfied

$$\frac{P}{\dot{R}_{\text{SNR}}^2} = \frac{3\beta \rho_{\text{ISM}}}{4} = \frac{B}{A^2} = \frac{\rho_{\text{ISM}} C_m}{2} \ .$$

This implies $C_m = \frac{3\beta}{2}$. Eq. (A6) can be simplified as

$$\frac{3E}{4\pi} = \rho_{\text{ISM}} C_e A^2 + \frac{3C_m \rho_{\text{ISM}} A^2}{4} = \rho_{\text{ISM}} \left(C_e + \frac{3C_m}{4} \right) \frac{4\alpha E}{25\rho_{\text{ISM}}} = \left(C_e + \frac{3C_m}{4} \right) \frac{4\alpha E}{25} \ , \quad (\text{A8})$$

and consequently

$$\frac{3}{4\pi} = \left(C_e + \frac{3C_m}{4} \right) \frac{4\alpha}{25} . \quad (\text{A9})$$

This allows us to obtain the coefficient as

$$C_e = \frac{75}{16\pi\alpha} - \frac{3C_m}{4} = \frac{75}{16\pi\alpha} - \frac{9\beta}{8} . \quad (\text{A10})$$

This means that the dynamic model can correctly reproduce the size of SNR and pressure of the gas at the explosion point if $C_m = \frac{3\beta}{2} \approx 0.45$, $C_e = \frac{75}{16\pi\alpha} - \frac{9\beta}{8} \approx 0.82$. The parameters $\alpha \approx 1.29$ and $\beta \approx 0.3$ are the numerical coefficients for the Sedov’s solution in politropic gas with $\gamma = 5/3$. The obtained values for C_e and C_m are also used in the dynamic model for the composite “PWN+SNR” model.

B. DIMENSIONLESS FORM OF EQUATIONS

The dimensionless equations that determine the expansion of the SNR and PWN are

$$\frac{dp}{d\tau} = \frac{5x^2a - 8(b_1 + b_2/s)}{(4 + x^3)r_{\text{SNR}}} , \quad (\text{B11})$$

$$\frac{dr_{\text{PWN}}}{d\tau} = \frac{(1 - x^3)a + 2x(b_1 + b_2/s)}{(4 + x^3)p} , \quad (\text{B12})$$

$$\frac{dv_{\text{SNR}}}{dt} = \frac{\frac{3ps}{C_m} - 3v_{\text{SNR}}^2}{r_{\text{SNR}}} , \quad (\text{B13})$$

$$\frac{dr_{\text{SNR}}}{d\tau} = v_{\text{SNR}} . \quad (\text{B14})$$

Here the characteristic time-, space- and energy-scales t_0 , R_0 , and L_0 define the dimensionless variables $t = t_0\tau$, $R_{\text{SNR}/\text{pwn}} = R_0 r_{\text{SNR}/\text{pwn}}$, $V_{\text{SNR}} = v_{\text{SNR}}(R_0/t_0)$, $P = \frac{L_0 t_0}{R_0^3} p$, $x = \frac{r_{\text{PWN}}}{r_{\text{SNR}}}$, $a = \frac{L}{4\pi L_0 r_{\text{PWN}}^2}$, $b_1 = v_{\text{SNR}} p \left(\frac{2C_e}{C_m} + \frac{3}{2} \right)$, and $b_2 = -C_e v_{\text{SNR}}^3$. Similarly to the Sedov’s solution, a dimensionless parameter

$$s = \frac{L_0 t_0^3}{\rho_{\text{ISM}} R_0^5} \quad (\text{B15})$$

accounts for the inertia of the ISM.

REFERENCES

- | | |
|--|--|
| Aharonian, F., et al. 2006, A&A, 460, 365 | Del Zanna, L., Amato, E., & Bucciantini, N. 2004, A&A, 421, 1063 |
| Aharonian, F. A., Atoyan, A. M., & Kifune, T. 1997, MNRAS, 291, 162 | Espinoza, C. M., Lyne, A. G., Kramer, M., Manchester, R. N., & Kaspi, V. M. 2011, ApJL, 741, L13 |
| Archibald, R. F., et al. 2016, ApJL, 819, L16 | Hamil, O., Stone, J. R., Urbanec, M., & Urbancová, G. 2015, PhRvD, 91, 063007 |
| Atoyan, A. M., & Aharonian, F. A. 1996, MNRAS, 278, 525 | Hamil, O., Stone, N. J., & Stone, J. R. 2016, PhRvD, 94, 063012 |
| Boyd, P. T., et al. 1995, ApJ, 448, 365 | Heger, A., Woosley, S. E., & Spruit, H. C. 2005, ApJ, 626, 350 |
| Bucciantini, N., Arons, J., & Amato, E. 2011, MNRAS, 410, 381 | Kargaltsev, O., Cerutti, B., Lyubarsky, Y., & Striani, E. 2015, SSRv, 191, 391 |
| de Jager, O. C., & Djannati-Ataï, A. 2009, in Astrophysics and Space Science Library, Vol. 357, Astrophysics and Space Science Library, ed. W. Becker, 451 | Kennel, C. F., & Coroniti, F. V. 1984a, ApJ, 283, 694 |
| de Jager, O. C., Funk, S., & Hinton, J. 2005, International Cosmic Ray Conference, 4, 239 | |

- . 1984b, *ApJ*, 283, 710
- Kolb, C., Blondin, J., Slane, P., & Temim, T. 2017, *ApJ*, 844, 1
- Livingstone, M. A., Kaspi, V. M., Gavriil, F. P., Manchester, R. N., Gotthelf, E. V. G., & Kuiper, L. 2007, *Ap&SS*, 308, 317
- Livingstone, M. A., Ng, C.-Y., Kaspi, V. M., Gavriil, F. P., & Gotthelf, E. V. 2011, *ApJ*, 730, 66
- Lyne, A. G., Pritchard, R. S., & Graham-Smith, F. 1993, *MNRAS*, 265, 1003
- Lyne, A. G., Pritchard, R. S., Graham-Smith, F., & Camilo, F. 1996, *Nature*, 381, 497
- Maceroni, C., Salvati, M., & Pacini, F. 1974, *Ap&SS*, 28, 205
- Mitchell, A. M. W., Caroff, S., Parsons, R. D., Hahn, J., Marandon, V., Hinton, J., & for the H. E. S. S. Collaboration. 2017a, *ArXiv e-prints*
- Mitchell, A. M. W., Mariaud, C., Eger, P., Funk, S., Hahn, J., Hinton, J., Parsons, R. D., & Marandon, V. 2017b, in *American Institute of Physics Conference Series*, Vol. 1792, 6th International Symposium on High Energy Gamma-Ray Astronomy, 040035
- Pacini, F., & Salvati, M. 1973a, *Astrophys. Lett.*, 13, 103
- . 1973b, *ApJ*, 186, 249
- Porth, O., Komissarov, S. S., & Keppens, R. 2014, *MNRAS*, 438, 278
- Rees, M. J., & Gunn, J. E. 1974, *MNRAS*, 167, 1
- Reynolds, S. P., & Chevalier, R. A. 1984, *ApJ*, 278, 630
- Rogers, A., & Safi-Harb, S. 2016, *MNRAS*, 457, 1180
- . 2017, *MNRAS*, 465, 383
- Roy, J., Gupta, Y., & Lewandowski, W. 2012, *MNRAS*, 424, 2213
- Stupar, M., Parker, Q. A., & Filipović, M. D. 2008, *MNRAS*, 390, 1037
- Van Etten, A., & Romani, R. W. 2011, *ApJ*, 742, 62
- Voisin, F., Rowell, G., Burton, M. G., Walsh, A., Fukui, Y., & Aharonian, F. 2016, *MNRAS*, 458, 2813
- Weltevredre, P., Johnston, S., & Espinoza, C. M. 2011, *MNRAS*, 411, 1917
- Zel'dovich, Y. B., & Raizer, Y. P. 1967, *Physics of shock waves and high-temperature hydrodynamic phenomena* (New York: Academic Press, 1966/1967, edited by Hayes, W.D.; Probstein, Ronald F.)